Terrestrial methane cycle perturbations during the onset of the Paleocene–Eocene Thermal Maximum

Gordon N. Inglis[1,2], Megan Rohrssen[3], Elizabeth M. Kennedy[4], Erica M. Crouch[4], J. Ian Raine[4], Dominic P. Strogen[4] , B. David A. Naafs[1], Margaret E. Collinson[5], and Richard D. Pancost[1]

[1] *Organic Geochemistry Unit, School of Chemistry and School of Earth Science, Cabot Institute for the Environment, University of Bristol, UK*

[2] *School of Ocean and Earth Science, University of Southampton, UK*

[3] *Geology and Environmental Sciences, Central Michigan University, USA*

[4] *Department of Surface Geosciences, GNS Science, Lower Hutt, New Zealand*

[5]*Department of Earth Sciences, Royal Holloway University of London, Egham, Surrey, UK*

Corresponding author: Gordon N. Inglis

Email: gordon.inglis@soton.ac.uk

ABSTRACT

Terrestrial methane (CH_4) emissions could have increased during the Paleocene–Eocene Thermal Maximum (~ 56 million years ago; Ma) and promoted additional warming, especially in the high latitudes. Although there is evidence for increased CH_4 cycling in a single Northern Hemisphere site, whether enhanced methane cycling was globally widespread is unknown as there have been no subsequent investigations. The mechanism of CH_4 release is also unknown because a direct comparison between temperature and CH_4 cycling has so far not been possible. Here we use biomarkers to reconstruct temperature change and CH_4 cycling in a new PETM-aged succession in New Zealand. Our results indicate that the stable carbon isotopic composition ($\delta^{13}C$) of bacterial hopanoids decreased to very low values (-60 ‰) during the onset of the PETM, indicating enhanced consumption of CH_4. These values are much lower than found in modern wetlands and suggest a major perturbation of the CH_4 cycle during the onset of the PETM. Low hopanoid $\delta^{13}C$ values do not persist into the early Eocene, despite evidence for elevated temperatures. This indicates that the terrestrial CH_4 cycle operates differently during transient compared to gradual warming events. Enhanced CH_4 cycling during the PETM may help to resolve the temperature data-model mismatch in the high-latitudes and could yield higher estimates of Earth system sensitivity than expected from CO_2 alone.

INTRODUCTION

The Paleocene-Eocene Thermal Maximum (PETM; ~56 Ma) is the most severe carbon cycle perturbation event of the Cenozoic. It is associated with ~5 °C of global warming (Dunkley Jones, 2013; Inglis et al., 2020) and an enhanced hydrological cycle (see Carmichael et al., 2017 and ref. therein), which are hypothesized to increase terrestrial CH_4 emissions (Beerling et al., 2011). Although this may have acted as an important positive feedback mechanism (Zeebe et al., 2009), there are few data to support this hypothesis.

The stable carbon isotopic composition ($\delta^{13}C$) of hopanoids (bacterial-derived biomarkers) can be used to reconstruct CH_4 cycling in peats (van Winden et al., 2012; Zheng et al., 2014) and lignites (Inglis et al., 2015; Pancost et al., 2007). Hopanoids are not exclusive to methanotrophs (Talbot and Farrimond, 2007), but can be linked to methanotrophy based on their $\delta^{13}C$ value (Freeman et al., 1990; Inglis et al., 2019b). Previous work from a single lignite deposit (Cobham, UK) revealed a dramatic decrease in hopanoid $\delta^{13}C$ values (minima: -75 ‰) during the onset of the PETM (Pancost et al., 2007). This suggested enhanced consumption of ^{13}C-depleted CH_4 during the onset of the PETM, potentially due to an increase in wetland methanogenesis and perhaps associated with an overall increase in CH_4 emissions. However, there have been no subsequent investigations of wetland CH_4 cycling during the PETM, in large part due to the paucity of such deposits. Moreover, the mechanism of CH_4 release remains uncertain because a direct comparison with temperature was not possible in the Cobham section (Inglis et al., 2019a).

Here we use biomarker data to reconstruct changes in temperature (branched glycerol dialkyl glycerol tetraethers; brGDGTs) and methanotrophy (hopanoid $\delta^{13}C$) from a new PETM-aged succession in Otaio River, New Zealand (~48°S paleolatitude). This novel dataset allows us

to explore: i) the relationship between temperature and CH_4 cycling and, ii) whether enhanced CH_4 cycling was widespread during the PETM.

MATERIALS AND METHODS

Depositional Setting

The Broken River Formation exposed in Otaio River (New Zealand; Fig. 1) consists of mixed sandstone, mudstone, and lignite facies (Fig. 2) and is overlain by the early Eocene Kauru Formation (Forsyth et al., 2001; Naafs et al., 2018; Pancost et al., 2013). The ~55m sequence sampled at Otaio River represents deposition in a low-energy, estuarine or deltaic setting with a change to marine deposition at ~41.5 m (Fig. 2). This marks the boundary between the Broken River and Kauru formations, as indicated by intense bioturbation, the presence of glauconite and abundant marine fauna (e.g. bivalves; Field and Browne, 1986; Marwick, 1960). The Broken River Formation also contains thin lignite seams (~10-50 cm thickness) which reflect a coastal wetland environment.

The sequence is thermally immature and characterised by high organic carbon content (~5%, but >30% in the lignites), high BIT indices (~0.6-1.0; Appendix 1), abundant terrestrial palynomorphs (Pancost et al., 2013) and abundant leaf wax biomarkers. Scattered leaf fossils also occur in mudstones from the lower part of the Broken River Formation exposure (Pancost et al., 2013). Collectively, this indicates a dominant input of terrestrial OM through the section.

Age Control

Sediments of the Broken River Formation are late Paleocene (NZ Teurian stage) to early Eocene (NZ Waipawan–Mangaorapan stages) age (~59 to 49.3 Ma) and encompass the PETM (5.5 m to

~17.5m; Fig. 2) (Naafs et al., 2018; Pancost et al., 2013). Identification of the PETM is based on: (i) a negative carbon isotope excursion (CIE) in bulk OM (Fig. 2a) and leaf wax biomarkers (Fig. 2b), (ii) a change from Paleocene (New Zealand pollen zone PM3a) to earliest Eocene (pollen zone PM3b) palynofloral indicators, including the appearance of thermophilic taxa (Fig. 2; Naafs et al., 2018), (iii) a marine incursion immediately following the onset of the CIE, and (iv) the dominance of the dinoflagellate cyst genus *Apectodinium* (Pancost et al., 2013; Fig. 2) between 9.50 and 11.70m depth. The occurrence of dinoflagellate cyst *Rhombodinium subtile* – previously only found in samples dated as calcareous nannoplankton Zone NP10 (Crouch et al., 2001; Crouch et al., 2020) suggests a post-PETM deposition by 17.45m depth (Fig. 2).

Analytical Methods

We analysed 24 samples including both lignite and shallow marine interbeds. Approximately 1-10g of sediment was extracted via Soxhlet apparatus for 24 hours using dichloromethane (DCM):methanol (MeOH) (2:1 *v/v*). The total lipid extract was separated over alumina into apolar and polar fractions using hexane:DCM (9:1 *v/v*) and DCM:MeOH (1:2 *v/v*), respectively. Urea adduction was performed upon the apolar fraction to separate non-adduct and adduct fractions (Pancost et al., 2008). Both fractions were analysed using a Thermo ISQ Single Quadrupole gas chromatography-mass spectrometer (GC-MS) and an Isoprime 100 GC-combustion-isotope ratio-MS system (Appendix 1). The polar fraction was dissolved in hexane/isopropanol (99:1, *v/v*), passed through 0.45μm PTFE filters and analysed by HPLC/APCI-MS using the methods of Hopmans et al. (2016).

RESULTS

Carbon cycling during the PETM

Bulk OM (Fig. 2a) and long-chain *n*-alkanes (Fig. 2b) exhibit a negative CIE during the onset of the PETM (ca. -2 and -3‰, respectively) and remain low throughout the early Eocene. The *n*-alkane CIE is similar to other terrestrial sites (e.g. Baczynski et al., 2019). There is no clear return to pre-PETM values, implying a hiatus between the PETM and early Eocene sediments (Fig. 2). This could be explained by low sample resolution and/or missing exposure between ~13 and 18m (Fig. 2). $\delta^{13}C$ values were also obtained for a range of hopanoids (i.e. C_{30} hop-17(21)-ene, C_{29} ββ hopane, and C_{31} αβ hopane). During the PETM, hop-17(21)-ene $\delta^{13}C$ values decrease from -31 to -61‰ (Fig. 2c). These values are lower than those observed in any modern peatland (-20 to -45‰; Inglis et al., 2019b). C_{29} ββ hopane $\delta^{13}C$ values exhibit similar temporal trends (Fig. 2c) and decrease from -35‰ to values as low as -43‰. C_{31} αβ hopane $\delta^{13}C$ values remain relatively invariant throughout the record, ranging between -25 and -32‰ (Fig. 2c). This is consistent with modern observational evidence, which indicates that C_{31} hopanoids are less sensitive tracers for methanotrophy (Inglis et al., 2019b).

Temperature change during the PETM

For lignites (TOC >20%) and coastal marine interbeds (TOC <5%), we translate brGDGT distributions into mean annual air temperature (MAAT) using a Bayesian calibration model ($BayMBT_0$; Crampton-Flood et al., 2020) (Appendix 1). During the body of the PETM, MAAT estimates from the marine interbeds increase from ~12 to 17 °C (Fig. 2e), consistent with the first occurrence of thermophilic taxa during the PETM. There is also an increase in MAAT estimates within the lignite beds from ~22 to 25°C (Fig. 2f), although only one lignite bed was recovered during the PETM. As such, the magnitude of warming (ca. 3°C) is a minimum estimate. The onset of warming in the marine interbeds occurs ~2m after the onset of the CIE. This could arise from

our relatively low sample resolution. Alternatively, it could arise from caveats associated with the brGDGT paleothermometer. For instance, recent work demonstrates that brGDGTs typically underestimate terrestrial temperatures within coastal marine settings (e.g. Inglis et al., 2017; Hollis et al., 2019). MAAT estimates from the marine interbeds and lignites yield different absolute values. This is attributed to changes in brGDGT provenance, as documented elsewhere (Inglis et al., 2017). Despite this, MAAT estimates from the lignites and marine interbeds yield a similar magnitude of warming (~3 to 5 °C) during the PETM (Fig. 2e-f). Following the PETM, MAAT estimates remain relatively high and stable (Fig. 2e-f).

DISCUSSION

Enhanced CH_4 cycling during the PETM at Otaio River

The $\Delta^{13}C_{hop\text{-}alk}$ index (= $\delta^{13}C_{hopanoid}$ - $\delta^{13}C_{alkane;}$ following Inglis et al. 2019b) has been developed to assess past variations in the CH_4 cycle. In modern wetlands, $\Delta^{13}C_{hop\text{-}alk}$ values range between +10 and -10‰. Here we calculate $\Delta^{13}C_{hop\text{-}alk}$ values using the C_{29} *n*-alkane, but similar results are obtained with other long-chain *n*-alkanes. Prior to the PETM, values in Otaio River (Fig. 2d) are similar to those observed in modern wetlands (Inglis et al., 2019b) and indicate a bacterial community largely consuming ^{13}C-enriched plant biomass. However, $\Delta^{13}C_{hop\text{-}alk}$ values (-15 to -30‰; Fig. 2d) during the onset of the PETM are far below the modern range (+10 to -10‰). Enhanced consumption of ^{13}C-depleted substrates (e.g. lipids, lignin) by heterotrophic bacteria could yield lower $\Delta^{13}C_{hop\text{-}alk}$ values during the onset of the PETM (Hobbie and Werner, 2004). However, in modern settings, the $\delta^{13}C$ value of the aforementioned substrates is rarely < -40 ‰ (Inglis et al., 2019). This implies that very low $\Delta^{13}C_{hop\text{-}alk}$ can only be explained by invoking the consumption of lighter substrates (i.e. CH_4). Within the body of the PETM (~9 to 17.5m; Fig. 2d),

$\Delta^{13}C_{hop\text{-}alk}$ values gradually return to pre-PETM values. These values persist into the early Eocene (~17.5m to 36m; Fig. 2d), despite persistently high MAATs and indicate that perturbations to the CH_4 cycle were limited to the onset of the PETM, similar to that observed at Cobham (Pancost et al., 2007).

Decoupling between physical climate and the CH_4 cycle during the PETM

Earth system model (ESM) simulations indicate coupling of physical climate processes (e.g. temperature, hydrology) under increasing CO_2 (e.g. Carmichael et al., 2016). However, perturbations in physical climate can trigger a cascade of biogeochemical feedbacks (e.g. enhanced runoff can increase the delivery of freshwater, nutrients and terrigenous materials to continental shelves with associated impacts on marine biogeochemistry; Carmichael et al., 2017). In our study, decoupling between physical climate (brGDGT-based MAAT) and the CH_4 cycle ($\delta^{13}C_{hopanoid}$) could arise from a range of factors. An increase in CO_2 could stimulate CH_4 emissions by increasing primary productivity (Beerling et al. 2011) and/or modifying substrate supply for methanogenesis (Yvon-Durocher et al., 2014). Although the PETM is characterized by higher CO_2 estimates compared to the EECO and late Paleocene (Hollis et al, 2019), CO_2 estimates from all three intervals remain poorly constrained. Alternatively, hopanoid $\delta^{13}C$ values and temperature could be related (e.g. Pancost et al., 2007), with higher temperatures leading to higher rates of methanogenesis (Yvon-Durocher et al., 2014) and therefore a larger methanotroph community and lower hopanoid $\delta^{13}C$ values. High temperatures (>20°C; Fig. 2e-f) and thermophilic taxa persist throughout the PETM and early Eocene. However, depleted hopanoid $\delta^{13}C$ values are limited to the PETM onset (Fig. 2c-d). The onset of warming (Fig. 2e-f) also appears to occur after the initial decline in hopanoid $\delta^{13}C$. Collectively, this indicates that temperature is not the primary control

185 regulating hopanoid $\delta^{13}C$ values at Otaio River. This is consistent with published studies that failed
186 to detect low hopanoid $\delta^{13}C$ values in Paleocene or early Eocene lignites, deposited under
187 greenhouse conditions (Diefendorf et al., 2015; Inglis et al., 2015; Fig. 3). Wetter and/or drier
188 conditions can also be associated with low hopanoid $\delta^{13}C$ values (Zheng et al., 2014). Although
189 the response of the hydrological cycle at Otaio River remains uncertain, nearby records indicate
190 an unstable hydrological cycle characterised by wet/dry cycles (Handley et al., 2011; Pole, 2010)
191 which could also have perturbed the wetland CH_4 cycle. Regardless of the primary forcing, the
192 striking observation from both Cobham and Otaio River is that the CH_4 cycle response was
193 dramatic but transient.
194
195 **Significance of enhanced CH_4 cycling in warm climates**
196 ESMs that include climate-chemistry feedbacks indicate that enhanced CH_4 emissions can
197 contribute ~20% of additional warming for a PETM-type event (i.e. a doubling of CO_2; Beerling
198 et al., 2011). Due to polar amplification, this may be even greater in the high-latitudes (Beerling
199 et al., 2011) and can reduce the high latitude temperature data-model mismatch (Hollis et al.,
200 2019). The inclusion of climate-chemistry feedbacks in an Eocene ESM (Beerling et al., 2011)
201 also leads to higher estimates of Earth system sensitivity (4.0°C) (i.e. the temperature rise resulting
202 from a doubling in CO_2 incorporating 'slow' and 'fast' feedbacks) than expected from CO_2 forcing
203 alone (3.2 °C; Beerling et al., 2011). ESMs that do not account for CH_4 emissions may therefore
204 underestimate Earth system sensitivity during the geological record.
205 We find no evidence for wetland CH_4 cycle perturbations during gradual warming events
206 (e.g. the early Eocene), implying that enhanced CH_4 emissions could be driven by the wider
207 geographical distribution of wetland environments (Beerling et al., 2011). This is consistent with

a two- to threefold increase in model-predicted wetland extent during the early Eocene (Wilton et al., 2019). Instead, perturbations in the terrestrial CH_4 cycle (Pancost et al., 2007; *this study*) appear to occur exclusively during climate transitions (e.g. the onset of the PETM). After the initial perturbation, the Earth system appears to stabilize (i.e. the body of the PETM), resulting in a climate regime that no longer favors CH_4 cycling. This demonstrates that the response of the CH_4 cycle is different for transient vs gradual warming events, and highlights the limitations of ESMs that simulate 'equilibrium' or steady state conditions (e.g. Beerling et al., 2011; Carmichael et al., 2016; Inglis et al., 2019a).

CONCLUSIONS

Here we reconstruct temperature change and CH_4 cycling in a new PETM-aged succession in Otaio River, New Zealand. Hopanoid $\delta^{13}C$ values during the onset of the PETM are much lower than observed today and indicate enhanced consumption of ^{13}C-depleted CH_4. These results indicate that a global perturbation of the CH_4 cycle occurred at the onset of the PETM. Low hopanoid $\delta^{13}C$ values do not persist into the early Eocene despite continuous high MAAT, indicating partial decoupling between physical climate and the CH_4 cycle. Enhanced CH_4 cycling during the PETM could help to resolve the temperature data-model mismatch in the high-latitudes and could yield higher estimates of Earth system sensitivity than expected from CO_2 alone. The dramatic but transient responses observed here could also foreshadow changes that the CH_4 cycle will experience in the future due to anthropogenic emissions.

ACKNOWLEDGMENTS

We thank three anonymous reviewers for constructive and helpful feedback. This research is funded via the ERC (340923) and NERC (NE\J008591\1). RDP acknowledges a Royal Society Wolfson Research Merit Award. GNI acknowledges a Royal Society Dorothy Hodgkin Fellowship (DHF\R1\191178). BDAN acknowledges a Royal Society Tata University Research Fellowship. GNI thanks H. Whelton and NEIF for analytical support and E. Dearing Crampton-Flood for generating BayMBT values. EMK, JIR, EMC and DPS were supported by the 'Global Change Through Time' programme at GNS Science.

Figure 1: Map of New Zealand showing the location of Otaio River (star).

Figure 2: CH_4 cycle perturbations at Otaio River during the PETM. 2a) bulk OM $\delta^{13}C$ values, 2b) C_{29} (black) and C_{31} (dark grey) *n*-alkane $\delta^{13}C$ values, 2c) C_{30} hop-17(21)-ene (black square), C_{29} ββ hopane (dark grey diamond) and C_{31} αβ hopane (light grey triangle) $\delta^{13}C$ values, 2d) C_{30} hop-17(21)-ene (black square), C_{29} ββ hopane (dark grey diamond) and C_{31} αβ hopane (light grey triangle) $\Delta^{13}C_{hop\text{-}alk}$ values, 2e) MAAT estimates in marine interbeds, and 2f) MAAT estimates in lignite seams. The shaded region in (2e) and (2f) indicates the 1σ error. Key biostratigraphic markers also shown (Pancost et al., 2013; Naafs et al., 2018).

Figure 3: $\Delta^{13}C_{hop\text{-}alk}$ values in a) mid-to-late Paleocene (63-56 Ma; Diefendorf et al., 2015; this paper), b) PETM (56 Ma; Pancost et al., 2007; this paper) and c) early Eocene (56-48 Ma; Diefendorf et al., 2015; Inglis et al., 2015; this paper) lignite and siliciclastic sediments.

REFERENCES

253 Baczynski, A.A., McInerney, F.A., Freeman, K.H., Wing, S.L. and Bighorn Basin Coring Project
254 (BBCP) Science Team, 2019. Carbon Isotope Record of Trace n-alkanes in a Continental
255 PETM Section Recovered by the Bighorn Basin Coring Project
256 (BBCP): Paleoceanography and Paleoclimatology, v. *34*, p.853-865.
257 Beerling, D. J., Fox, A., Stevenson, D. S., and Valdes, P. J., 2011, Enhanced chemistry-climate
258 feedbacks in past greenhouse worlds: Proceedings of the National Academy of Sciences,
259 v. 108, no. 24, p. 9770-9775.
260 Carmichael, M.J., Lunt, D.J., Huber, M., Heinemann, M., Kiehl, J., LeGrande, A., Loptson, C.A.,
261 Roberts, C.D., Sagoo, N., Shields, C., Valdes, P.J., Winguth, A., Winguth, C., and Pancost,
262 R.D., 2016, A model–model and data–model comparison for the early Eocene hydrological
263 cycle: Climate of the Past, v. 12, p. 455-481.
264 Carmichael, M. J., Inglis, G. N., Badger, M. P., Naafs, B. D. A., Behrooz, L., Remmelzwaal, S.,
265 Monteiro, F. M., Rohrssen, M., Farnsworth, A., and Buss, H. L., 2017, Hydrological and
266 associated biogeochemical consequences of rapid global warming during the Paleocene-
267 Eocene Thermal Maximum: Global and Planetary Change, v. 157, p. 114-138.
268 Crampton-Flood, E. D., Tierney, J. E., Peterse, F., Kirkels, F. M., and Damsté, J. S. S., 2020,
269 BayMBT: A Bayesian calibration model for branched glycerol dialkyl glycerol tetraethers
270 in soils and peats: Geochimica et Cosmochimica Acta, v. 268, p. 142-159.
271 Crouch E.M., Morgans H.E.G., Shepherd C.L., Naafs B.D.A., Dallanave E., Philips A., Hollis
272 C.J., Pancost R. 2020. Climatic and environmental change across the Early Eocene
273 Climatic Optimum at mid-Waipara River, Canterbury Basin, New Zealand. Earth Science
274 Reviews, 200, 102961

Crouch, E.M., 2001. Environmental Change at the Time of the Paleocene–Eocene Biotic Turnover. (PhD thesis) LPP contribution series, 14. Utrecht University, Utrecht, 90-393-2828-5.

Diefendorf, A. F., Freeman, K. H., Wing, S. L., Currano, E. D., and Mueller, K. E., 2015, Paleogene plants fractionated carbon isotopes similar to modern plants: Earth and Planetary Science Letters, v. 429, p. 33-44.

Dunkley-Jones, T., Lunt, D. J., Schmidt, D. N., Ridgwell, A., Sluijs, A., Valdes, P. J., and Maslin, M., 2013, Climate model and proxy data constraints on ocean warming across the Paleocene–Eocene Thermal Maximum: Earth Science Reviews, v. 125, p. 123-145.

Field, B., and Browne, G., 1986, Lithostratigraphy of Cretaceous and Tertiary rocks, southern Canterbury, New Zealand: New Zealand Geological Survey.

Forsyth, P., Glassey, P., and Barrell, D., 2001, Geology of the Waitaki area (1:250 000 geological map), Institute of Geological & Nuclear Sciences, Institute of Geological & Nuclear Sciences.

Freeman, K.H., Hayes, J.M., Trendel, J.-M., Albrecht, P., 1990. Evidence from carbon isotope measurements for diverse origins of sedimentary hydrocarbons. Nature, v. 343, p. 254-256

Handley, L., Crouch, E. M., and Pancost, R. D., 2011, A New Zealand record of sea level rise and environmental change during the Paleocene–Eocene Thermal Maximum: Palaeogeography, Palaeoclimatology, Palaeoecology, v. 305, no. 1-4, p. 185-200.

Hobbie, E.A. and Werner, R.A., 2004. Intramolecular, compound-specific, and bulk carbon isotope patterns in C3 and C4 plants: a review and synthesis. New Phytologist, v. 161, p. 371-385.

297 Hollis, C. J., Dunkley Jones, T., Anagnostou, E., Bijl, P. K., Cramwinckel, M. J., Cui, Y., Dickens,
298 G. R., Edgar, K. M., Eley, Y., Evans, D., Foster, G. L., Frieling, J., Inglis, G. N., Kennedy,
299 E. M., Kozdon, R., Lauretano, V., Lear, C. H., Littler, K., Lourens, L., Meckler, A. N.,
300 Naafs, B. D. A., Pälike, H., Pancost, R. D., Pearson, P. N., Röhl, U., Royer, D. L.,
301 Salzmann, U., Schubert, B. A., Seebeck, H., Sluijs, A., Speijer, R. P., Stassen, P., Tierney,
302 J., Tripati, A., Wade, B., Westerhold, T., Witkowski, C., Zachos, J. C., Zhang, Y. G.,
303 Huber, M., and Lunt, D. J., 2019, The DeepMIP contribution to PMIP4: methodologies for
304 selection, compilation and analysis of latest Paleocene and early Eocene climate proxy
305 data, incorporating version 0.1 of the DeepMIP database: Geoscientific Model
306 Development, v. 12, no. 7, p. 3149-3206.
307 Hopmans, E. C., Schouten, S., and Damsté, J. S. S., 2016, The effect of improved chromatography
308 on GDGT-based palaeoproxies: Organic Geochemistry, v. 93, p. 1-6.
309 Inglis, G. N., Collinson, M. E., Riegel, W., Wilde, V., Farnsworth, A., Lunt, D. J., Valdes, P.,
310 Robson, B. E., Scott, A. C., and Lenz, O. K., 2017, Mid-latitude continental temperatures
311 through the early Eocene in western Europe: Earth and Planetary Science Letters, v. 460,
312 p. 86-96.
313 Inglis, G. N., Collinson, M. E., Riegel, W., Wilde, V., Robson, B. E., Lenz, O. K., and Pancost, R.
314 D., 2015, Ecological and biogeochemical change in an early Paleogene peat-forming
315 environment: linking biomarkers and palynology: Palaeogeography, Palaeoclimatology,
316 Palaeoecology, v. 438, p. 245-255.
317 Inglis, G. N., Farnsworth, A., Collinson, M. E., Carmichael, M. J., Naafs, B. D. A., Lunt, D. J.,
318 Valdes, P. J., and Pancost, R. D., 2019a, Terrestrial environmental change across the onset

of the PETM and the associated impact on biomarker proxies: A cautionary tale: Global and Planetary Change, v. 181, p. 102991.

Inglis, G. N., Naafs, B. D. A., Zheng, Y., Schellekens, J., and Pancost, R. D., 2019b, δ13C values of bacterial hopanoids and leaf waxes as tracers for methanotrophy in peatlands: Geochimica et Cosmochimica Acta. v 260. p. 244-256

Inglis, G.N., Bragg, F., Burls, N., Cramwinckel, M.J., Evans, D., Foster, G.L., Huber, M., Lunt, D.J., Siler, N., Steinig, S., Tierney, J.E., Wilkinson, R., Anagnostou, E., de Boer, A.M., Dunkley Jones, T., Edgar, K., Hollis, C.J., Hutchinson, D.K and Pancost, R.D, 2020, Global mean surface temperature and climate sensitivity of the EECO, PETM and latest Paleocene: Climate of the Past Discussions. https://doi.org/10.5194/cp-2019-167.

Marwick, J., 1960, Early Tertiary Mollusca from Otaio Gorge South Canterbury, Department of Scientific and Industrial Research, New Zealand Geological Survey.

Naafs, B., Rohrssen, M., Inglis, G., Lähteenoja, O., Feakins, S., Collinson, M., Kennedy, E., Singh, P., Singh, M., and Lunt, D., 2018, High temperatures in the terrestrial mid-latitudes during the early Palaeogene: Nature Geoscience, v. 11, no. 10, p. 766.

Pancost, R. D., Baas, M., van Geel, B., and Sinninghe Damsté, J. S., 2003, Response of an ombrotrophic bog to a regional climate event revealed by macrofossil, molecular and carbon isotopic data: The Holocene, v. 13, no. 6, p. 921-932.

Pancost, R. D., Coleman, J. M., Love, G. D., Chatzi, A., Bouloubassi, I., and Snape, C. E., 2008, Kerogen-bound glycerol dialkyl tetraether lipids released by hydropyrolysis of marine sediments: A bias against incorporation of sedimentary organisms?: Organic Geochemistry, v. 39, no. 9, p. 1359-1371.

Pancost, R. D., Steart, D. S., Handley, L., Collinson, M. E., Hooker, J. J., Scott, A. C., Grassineau, N. V., and Glasspool, I. J., 2007, Increased terrestrial methane cycling at the Palaeocene–Eocene thermal maximum: Nature, v. 449, no. 7160, p. 332.

Pancost, R. D., Taylor, K. W., Inglis, G. N., Kennedy, E. M., Handley, L., Hollis, C. J., Crouch, E. M., Pross, J., Huber, M., and Schouten, S., 2013, Early Paleogene evolution of terrestrial climate in the SW Pacific, Southern New Zealand: Geochemistry, Geophysics, Geosystems, v. 14, no. 12, p. 5413-5429.

Pole, M., 2010, Ecology of Paleocene-Eocene vegetation at Kakahu, South Canterbury, New Zealand: Palaeontologia Electronica, v. 13, no. 2, p. 29.

Talbot, H. M., Bischoff, J., Inglis, G. N., Collinson, M. E., and Pancost, R. D., 2016, Polyfunctionalised bio-and geohopanoids in the Eocene Cobham Lignite: Organic Geochemistry, v. 96, p. 77-92.

Talbot, H. M., and Farrimond, P., 2007, Bacterial populations recorded in diverse sedimentary biohopanoid distributions: Organic Geochemistry, v. 38, no. 8, p. 1212-1225.

Van Winden, J. F., Talbot, H. M., De Vleeschouwer, F., Reichart, G.-J., and Damsté, J. S. S., 2012, Variation in methanotroph-related proxies in peat deposits from Misten Bog, Hautes-Fagnes, Belgium: Organic Geochemistry, v. 53, p. 73-79.

Wilton, D. J., Badger, M. P. S., Kantzas, E. P., Pancost, R. D., Valdes, P. J., and Beerling, D. J., 2019, A predictive algorithm for wetlands in deep time paleoclimate models: Geoscientific Model Development, v. 12, no. 4, p. 1351-1364.

Yvon-Durocher, G., Allen, A. P., Bastviken, D., Conrad, R., Gudasz, C., St-Pierre, A., Thanh-Duc, N., and Del Giorgio, P. A., 2014, Methane fluxes show consistent temperature dependence across microbial to ecosystem scales: Nature, v. 507, no. 7493, p. 488-491.

364 Zeebe, R. E., Zachos, J. C., and Dickens, G. R., 2009, Carbon dioxide forcing alone insufficient to
365 explain Palaeocene–Eocene Thermal Maximum warming: Nature Geoscience, v. 2, no. 8,
366 p. 576-580.
367 Zheng, Y., Singarayer, J. S., Cheng, P., Yu, X., Liu, Z., Valdes, P. J., and Pancost, R. D., 2014,
368 Holocene variations in peatland methane cycling associated with the Asian summer
369 monsoon system: Nature communications, v. 5, p. 4631.
370
371 [1]GSA Data Repository item xxxx (i.e. bulk and compound-specific isotope data, biomarker
372 distributions), is available online at www.geosociety.org/pubs/ft20XX.htm, or on request from
373 editing@geosociety.org or Documents Secretary, GSA, P.O. Box 9140, Boulder, CO 80301, USA.
374

Figure 1

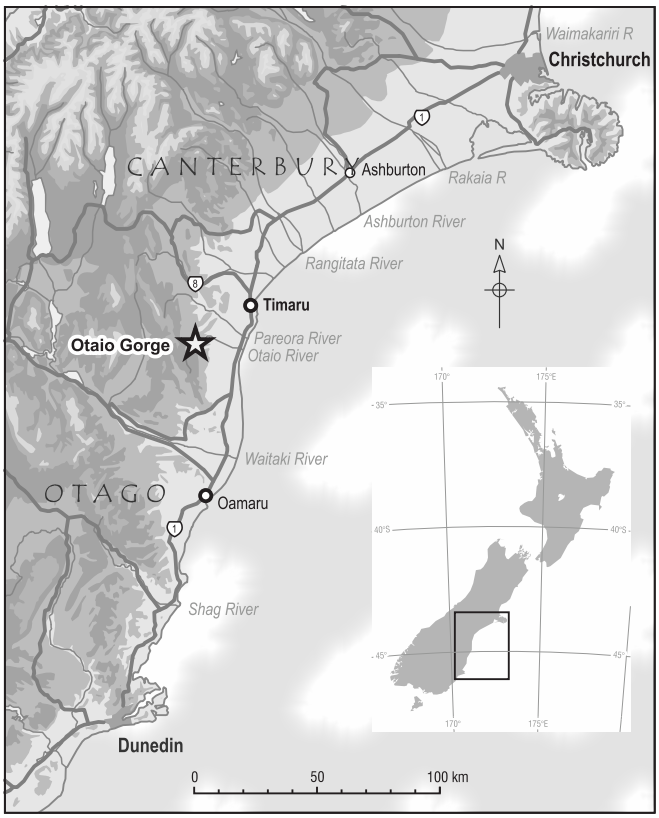
Waimakariri R
Christchurch
CANTERBURY
Ashburton
Rakaia R
Ashburton River
Rangitata River
N
Timaru
Otaio Gorge
Pareora River
Otaio River
Waitaki River
OTAGO
Oamaru
Shag River
Dunedin
0
50
100 km

Figure 2

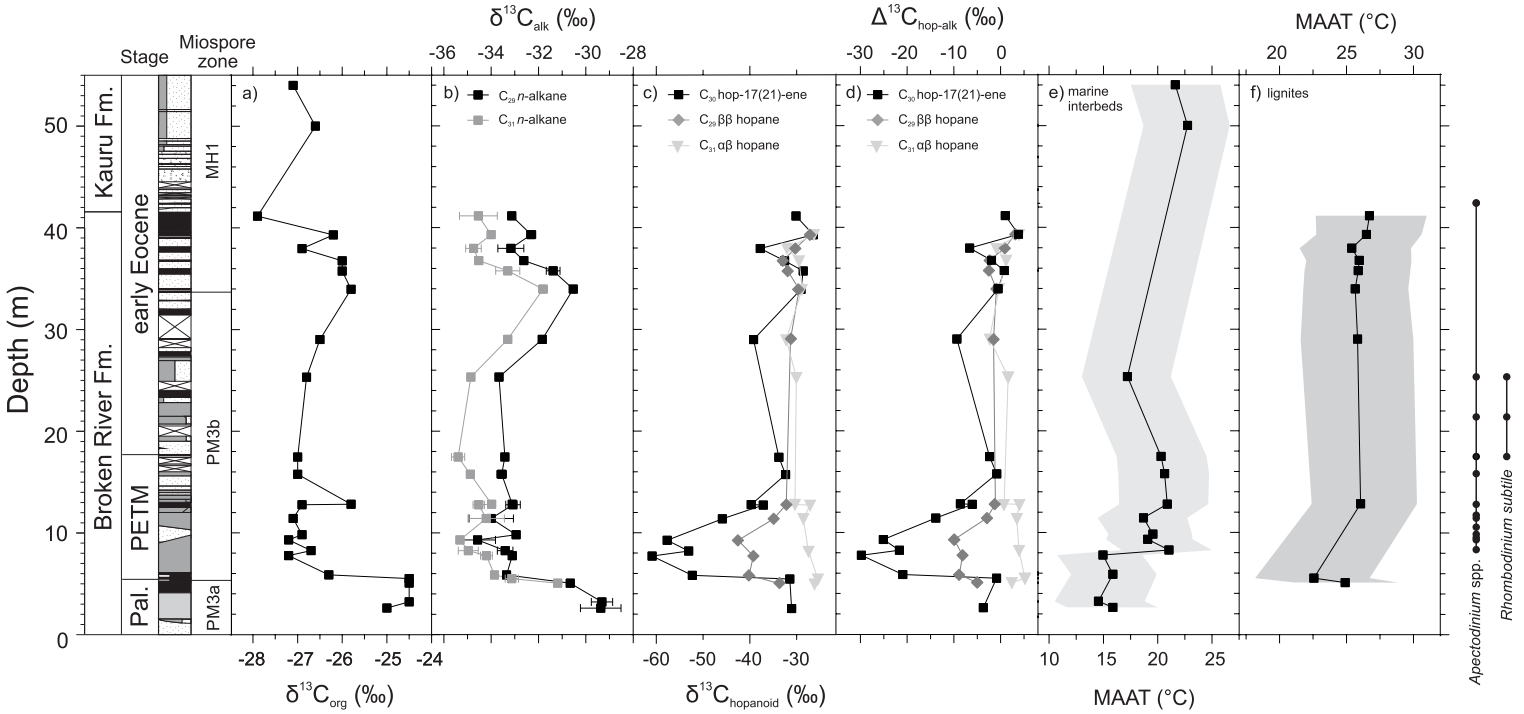
Stage
Miospore zone
Kauru Fm.
Broken River Fm.
early Eocene
PETM
Pal.
MH1
PM3b
PM3a
Depth (m)
δ13Calk (‰)
Δ13Chop-alk (‰)
MAAT (°C)
a)
b) C29 n-alkane
C31 n-alkane
c) C30 hop-17(21)-ene
C29 ββ hopane
C31 αβ hopane
d) C30 hop-17(21)-ene
C29 ββ hopane
C31 αβ hopane
e) marine interbeds
f) lignites
δ13Corg (‰)
δ13Chopanoid (‰)
MAAT (°C)
Apectodinium spp.
Rhombodinium subtile

Figure 3

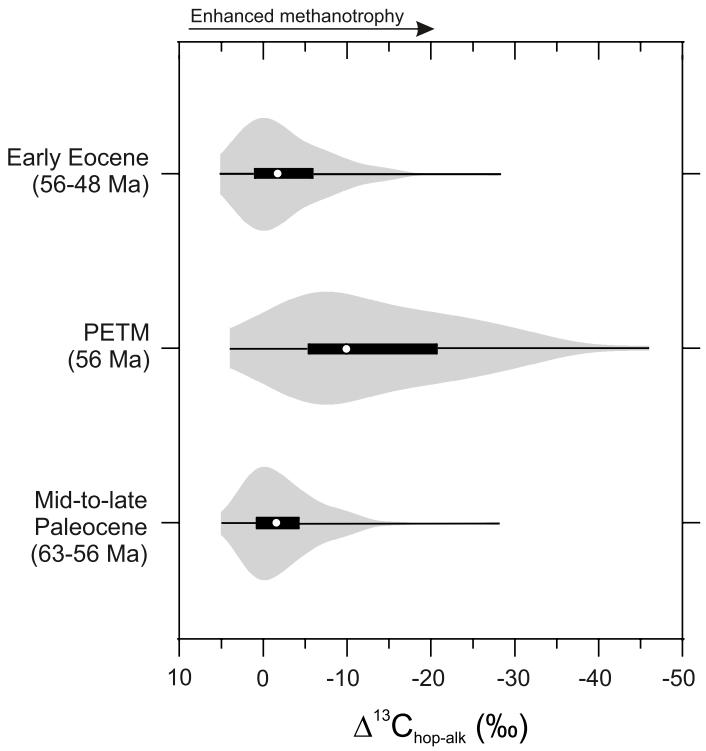
Enhanced methanotrophy
Early Eocene
(56-48 Ma)
PETM
(56 Ma)
Mid-to-late
Paleocene
(63-56 Ma)
10
0
-10
-20
-30
-40
-50
Δ13Chop-alk (‰)